Supporting Information for:

Efficient alkene hydrogenation over magnetically recoverable and recyclable Fe_3O_4@GO nanocatalyst using hydrazine hydrate as the hydrogen source

John Mondal,[a] Kim Truc Nguyen,[a] Avijit Jana,[a] Karina Kurniawan, [a] Parijat Borah,[a] Yanli Zhao*[ac] and Asim Bhaumik*[b]

[a]Division of Chemistry and Biological Chemistry, School of Physical and Mathematical Sciences, Nanyang Technological University, 21 Nanyang Link, Singapore 637371, zhaoyanli@ntu.edu.sg

[b] Department of Materials Science, Indian Association for the Cultivation of Science, Jadavpur 700 032, India, msab@iacs.res.in

[c]School of Materials Science and Engineering, Nanyang Technological University, 50 Nanyang Avenue, Singapore 639798

Table of Contents

Section S1: Characterization Techniques

X-ray diffraction (XRD) patterns were recorded on a Bruker D-8 Advance SWAX diffractometer operated at 40 kV voltage and 40 mA current. The instrument was calibrated with a standard silicon sample using Ni-filtered Cu K_α (α = 0.15406 nm) radiation. A JEOL JEM 6700F field emission scanning electron microscope (FE-SEM) was used for determining the morphology of the samples. Energy-dispersive X-ray spectroscopy (EDX pattern) and elemental mapping was carried out with this JEOL JEM 6700F machine. High resolution transmittance electron microscopic (HR-TEM) images were recorded in a JEOL JEM 2010 transmission electron microscope. Fe loading in the sample was estimated by using a Perkin-Elmer Optima 2100 DV Inductive Coupled Plasma Mass Spectroscopy (ICP-MS). Raman spectra on cleaned silicon substrate were measured with a Raman microscope (LabRAM HR, Horiba Yvon). The excitation wavelength of the irradiating light was 632.8 nm (He-Ne Laser, Melles Griot, laser excitation 0.1mW) and signals were collected by using × 50 objective lens. X-ray photoelectron spectroscopy (XPS) analysis was carried out by a SPECS I3500 plus spectrometer using Mg X-ray source. FT IR spectra of the samples were recorded using a Nicolet MAGNA-FT IR 750 Spectrometer Series II. Hydrodynamic diameter was determined by dynamic light scattering (DLS) with particle sizing software (90 plus, Brookhaven Instruments Co. USA) at a fixed angle of 90^o at room temperature. Atomic force microscopy (AFM) images were obtained using MultiMode 8 atomic force microscope with tapping mode and analyzed by Nano Scope Analysis program. Quadrupole ion trap Mass Spectrometer equipped with Thermo Accela LC and Agilent 6890 GC system equipped with a flame ionization detector were used for analysis of catalytic reactions.

Section S2: Experimental Procedure

Synthesis of Fe_3O_4@GO nanocatalysts:

GO dispersion (3 mL, 0.5 mg/mL in water), $FeCl_3$ (0.47 and 0.65 g, respectively), and DEG (40 mL) were mixed in a round bottom flask by sonication. Trisodium citrate (0.47 g, l.60 mmol) was added into the mixture and stirred at 80 °C until a clear brown solution was obtained. Subsequently, NaOAc (0.98 g, 11.95 mmol) was added. The mixture was kept stirring until everything completely dissolved. Hydrothermal process was carried out at 200 °C for 4 hours and 10 hours, respectively. The final product was washed several times with copious amount of EtOH by centrifugation at 7800 g for 10 minutes and dried to yield a fine brown powder of GO-Fe_3O_4. We have obtained the magnetic Fe_3O_4 nanoparticles (5 nm and 15 nm) embedded on graphene oxide in this method. The two nanocatalysts synthesized for 4 hr (with the size 5 nm) and 10 hr (with the 15 nm particle sizes) are designated as Fe_3O_4@GO-1 and Fe_3O_4@GO-2, respectively.

Catalytic Alkene hydrogenation with Fe_3O_4@GO nanocatalysts using hydrazine hydrate as hydrogen source:

In a typical catalytic alkene hydrogenation procedure a 25 mL sealed tube was charged with alkene (0.25 mmol) mixed with 5 mL absolute ethanol and Fe_3O_4@GO nanocatalysts (15 mg). Then catalyst was dispersed in the mixture by sonication thoroughly. Then hydrazine hydrate (10 equivalent, 2.5 mmol, 125 mg) was added dropwise into the previous reaction mixture. The tube was capped tightly and subjected to heat at 80^{o}C in an oil bath for the time referred. After the desired time interval reaction mixture was cooled at room temperature and catalyst was separated by magnetic separation. The reaction was monitored periodically by analyzing the reaction

mixture with GC-MS until the full conversion of substrate. The products were confirmed by employing GC-MS analysis technique. The conversions (%) of the products were determined by using dodecane as the internal standard.

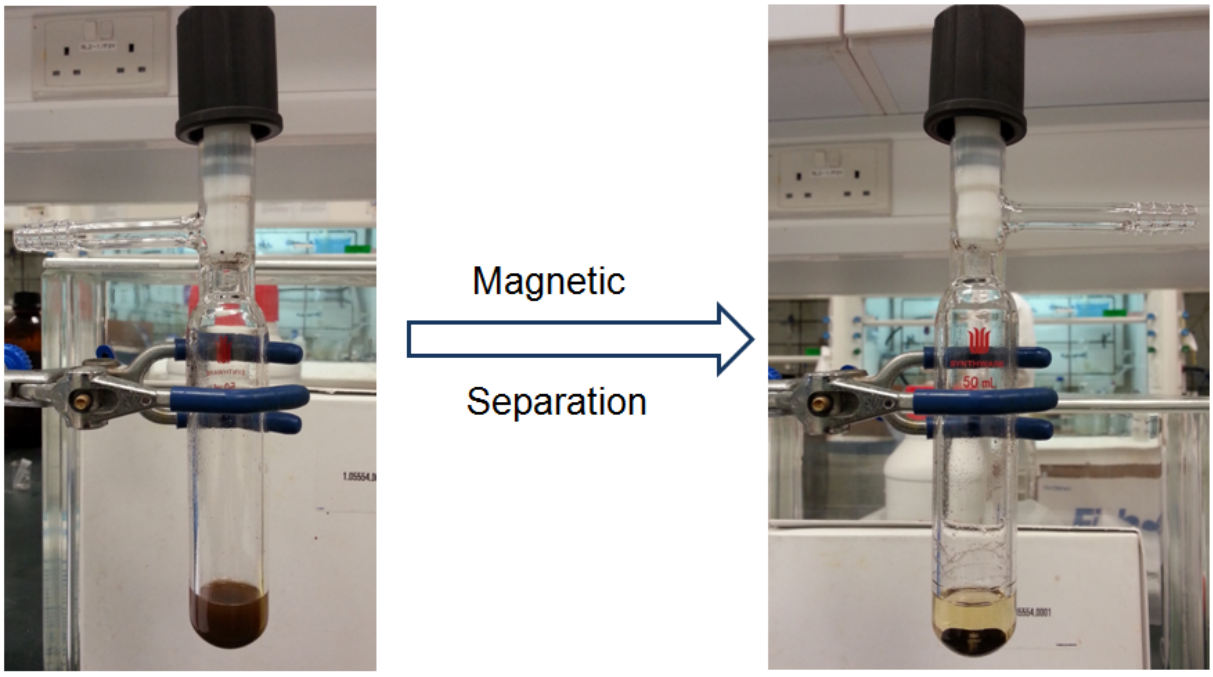

Uniqueness of Fe_3O_4@GO nanocatalyst synthesis procedure:

We believe that our synthesis procedure is novel based on the following reasons. (1) We have used optimized ratio of graphene oxide, $FeCl_3$, Na-Citrate and NaOAc to get the homogeneous size distribution of Fe_3O_4 nanoparticles and also homogeneous Fe_3O_4@GO nanocomposites. (2) We can control the size of Fe_3O_4 nanoparticles by controlling the reaction synthesis time in a facile one-pot synthesis procedure. (3) Very less expensive and easily available Fe-precursor

compared with expensive and moisture sensitive $Fe(CO)_5$ precursor has been used here to generate homogeneous distribution of Fe_3O_4 nanoparticles.[1a-b] (4) Previously reports based on the based on the *ex situ* synthesis of chemically stabilized magnetic particles with 2-nitrodopamine, followed by their insertion onto the GO matrix.[1c] (5) In this route Fe_3O_4 nanoparticles are prepared by following some water-dispersibility reagent due to a hydrophilic coating compared to the high temperature thermal decomposition method.[1d] (6) DEG acts as high boiling point solvent, reductant and as well as stabilizer to control the particle growth preventing them from aggregation.

Merits of Fe_3O_4@GO nanocatalyst and our newly developed methodology for alkene hydrogenation:

Merits of our catalysts lies in the synthesis and performing catalytic reactions. (1) Synthesis of catalysts can be achieved in a facile one-pot single step procedure with homogeneous distribution of Fe_3O_4 nanoparticles and Fe_3O_4@GO nanocomposites. (2) Very cheap and easily available materials are used to synthesis the catalysts and no multi steps are involved in our synthesis procedure. (3) Our catalyst is magnetically recoverable and no loss (100% catalyst recovery) took place during the course of separation for reusability test. (4) No extra procedure and reagents are required to reactivate our catalysts for next catalytic cycles. (5) Use of highly flammable H_2 gas at high pressure and temperature are not needed for our methodology. (6) Although the reaction times are quite long but we have achieved a high TOF value for each substrate and also our catalyst is more active compared with Pd/C catalyst under this conditions. (7) No leaching of Fe took place during the course of reaction. We believe that these are merits involved in our catalysts which are more helpful compared with Pd/C catalyst which often catches fire during the course of hydrogenation reaction using hydrogen balloon.

Preparation of Fe_3O_4@GO nanocatalyst in a facile one-pot procedure:

The possible mechanism and roles of sodium citrate and sodium acetate for the development of Fe_3O_4@GO nanocatalyst is predicted in the Scheme S1. Fe^{3+} ions from aqueous solution of $FeCl_3$ favourably bind with the carboxyl groups of graphene oxide nanosheets due to electrostatic interaction between Fe^{3+} ions and negatively charged carboxyl groups. At the same time Na citrate was added in the resulting $FeCl_3$-GO-DEG solution. DEG acts as high boiling point solvent, reductant and as well as stabilizer to control the particle growth preventing them from aggregation. As a result Fe(III)-citrate complex is formed owing to coordination of citrate ions and Fe(III) ions. Actually citrate ions behave as a capping agent in this case. NaOAc is used to make the solution alkaline. In the presence of DEG and Na_3Cit, Fe_3O_4 crystallites form firstly under alkaline condition, followed by further growth into Fe_3O_4 nanoparticles as the reaction time is prolonged in this system. As we have added Na citrate in excess so Na citrate will bind strongly on the surface of Fe_3O_4 nanoparticles and decreasing the size of Fe_3O_4 nanoparticles prohibiting them from agglomeration. [1e]

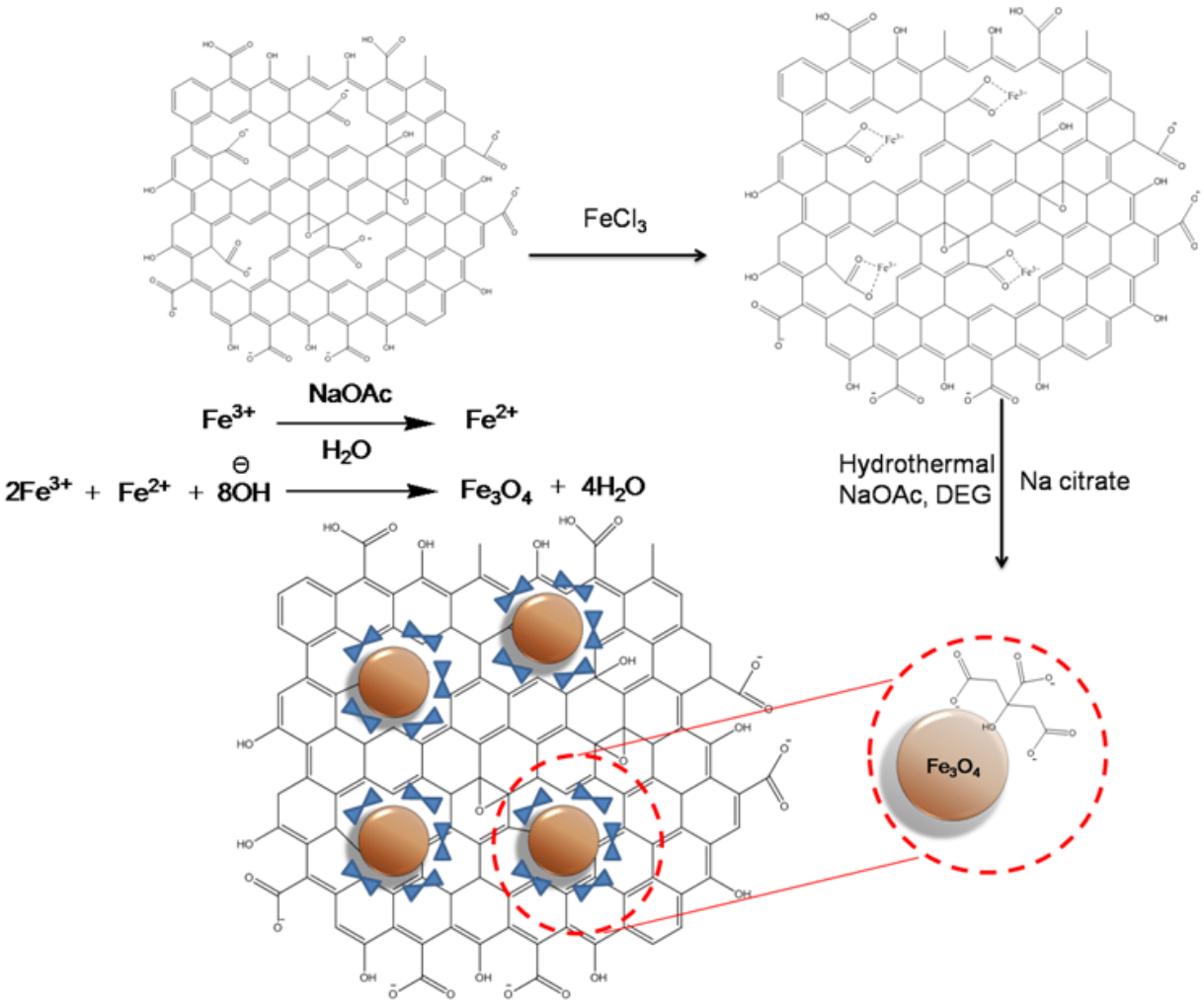

Scheme S1: Preparation of Fe_3O_4@GO nanocatalyst in a facile one-pot synthesis procedure.

Section S3: All TEM images of Fe_3O_4@GO-1 nanocatalyst

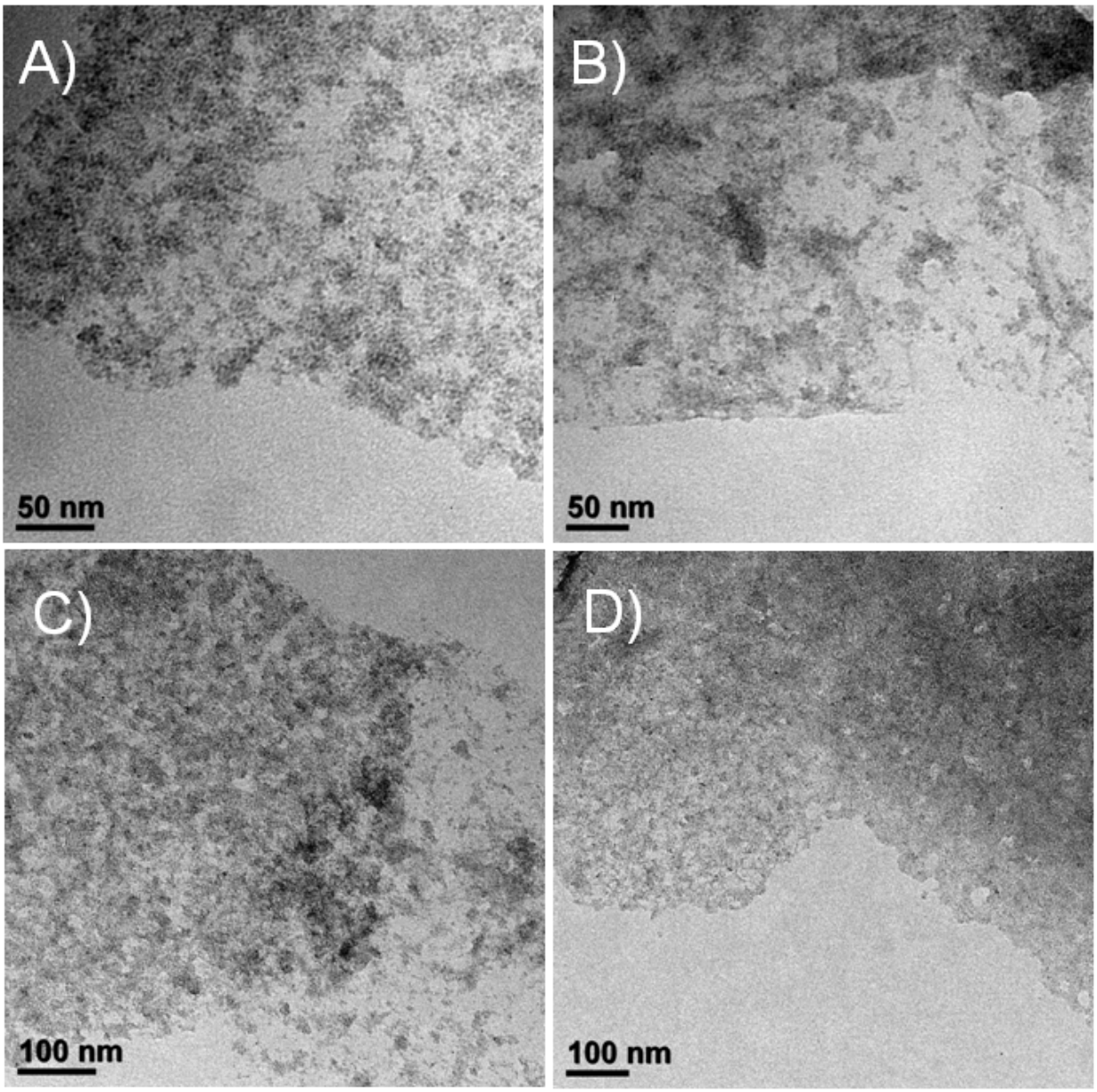

Figure S1: All TEM images (A, B, C & D) of Fe_3O_4@GO-1nanocatalyst

Section S4: All TEM images of Fe_3O_4@GO-2 nanocatalyst

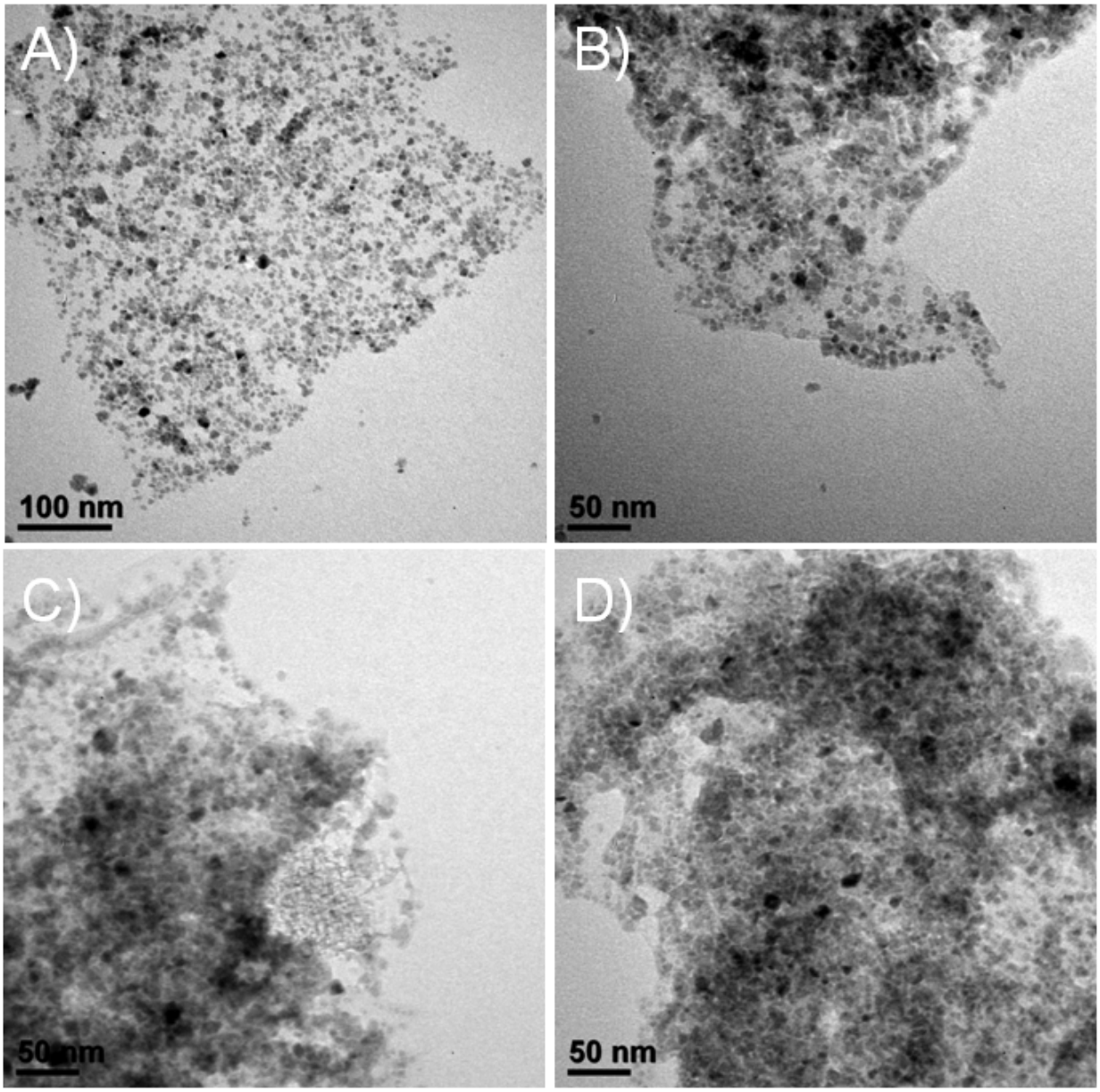

Figure S2: All TEM images (A, B, C & D) of Fe_3O_4@GO-2 nanocatalyst

TEM images of Fe_3O_4@GO-1 and Fe_3O_4@GO-2 nanocatalysts are provided in Figure S1 and Figure S2, respectively. All the images signify that the surfaces of graphene oxide are densely sheltered with homogeneously distributed black colored Fe_3O_4 nanoparticles with the sizes 5 nm

(Figure S1) and 15 nm (Figure S2), respectively. The distribution of Fe_3O_4 nanoparticles are distributed on each graphene oxide sheet in such a way so that no big agglomeralation of Fe_3O_4 or large vacancy on graphene oxide is observed.

Section S5: EDX pattern and elemental mapping of Fe_3O_4@GO-1 nanocatalyst

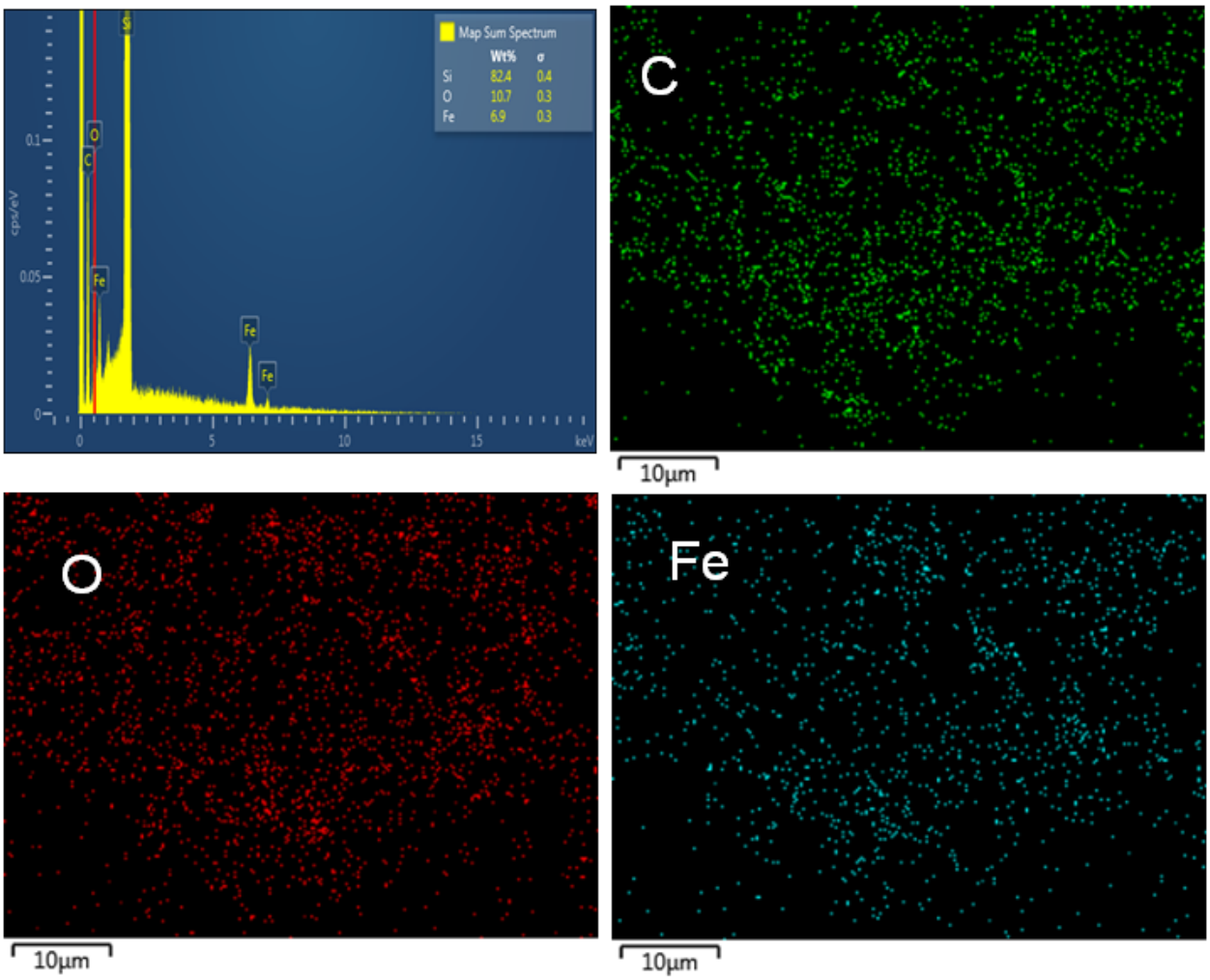

Figure S3: EDX spectrum analysis and corresponding elemental mapping **C**, **O** and **Fe** of Fe_3O_4@GO-1nanocatalyst

Section S6: EDX pattern and elemental mapping of Fe_3O_4@GO-2 nanocatalyst

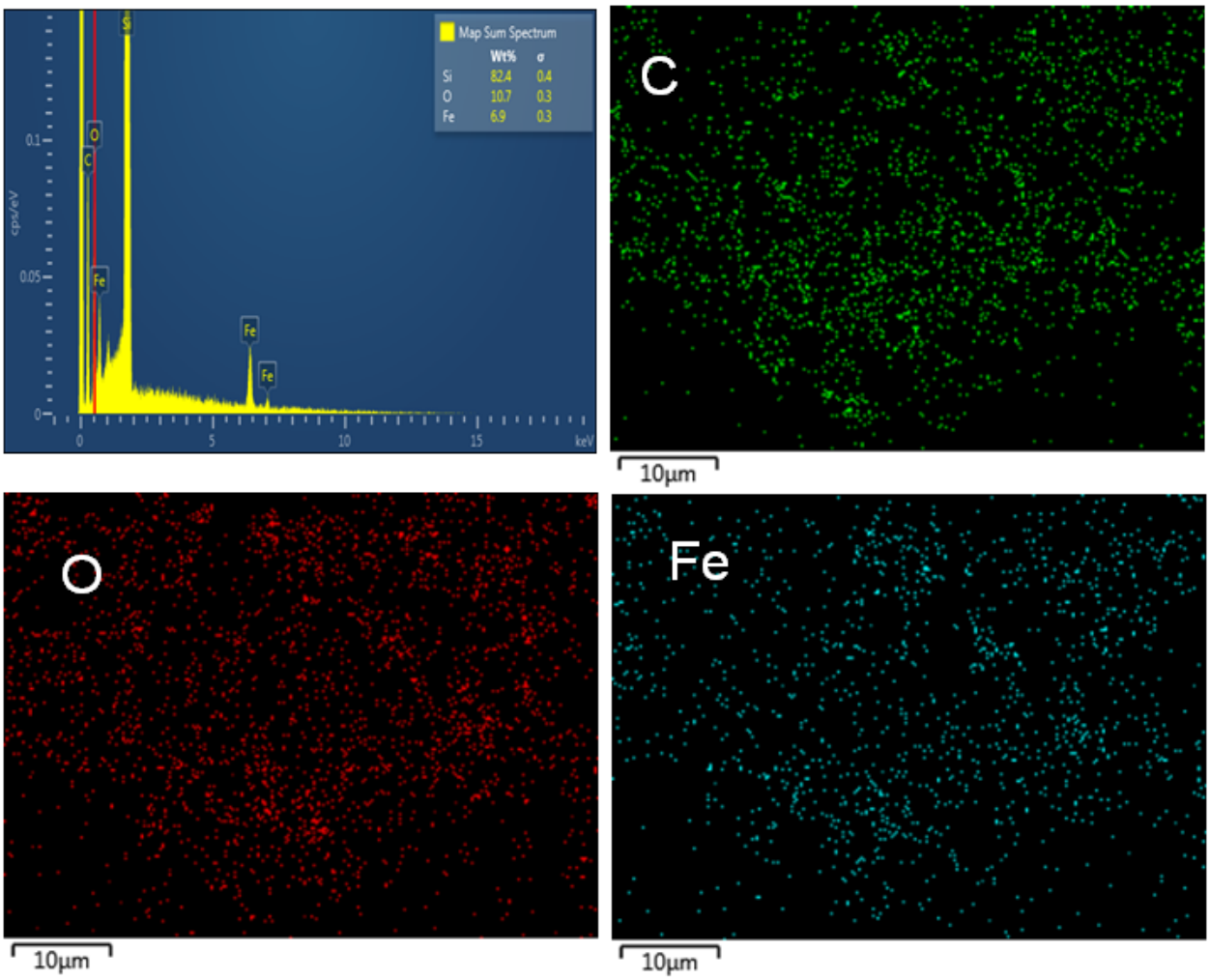

Figure S4: EDX spectrum analysis and corresponding elemental mapping **C**, **O** and **Fe** of Fe_3O_4@GO-2 nanocatalyst

We have carried out Energy Dispersive X-Ray (EDX pattern) and elemental mapping of C, O and Fe for Fe_3O_4@GO-1 and Fe_3O_4@GO-2 nanocatalysts, respectively (Figure S3 & S4). The images suggest that the homogenous distribution of C, O and Fe elements throughout the materials. And EDX pattern describes the presence of Fe in the nanocatalysts.

Section S7: Wide angle powder XRD patterns of Fe_3O_4@GO nanocatalysts

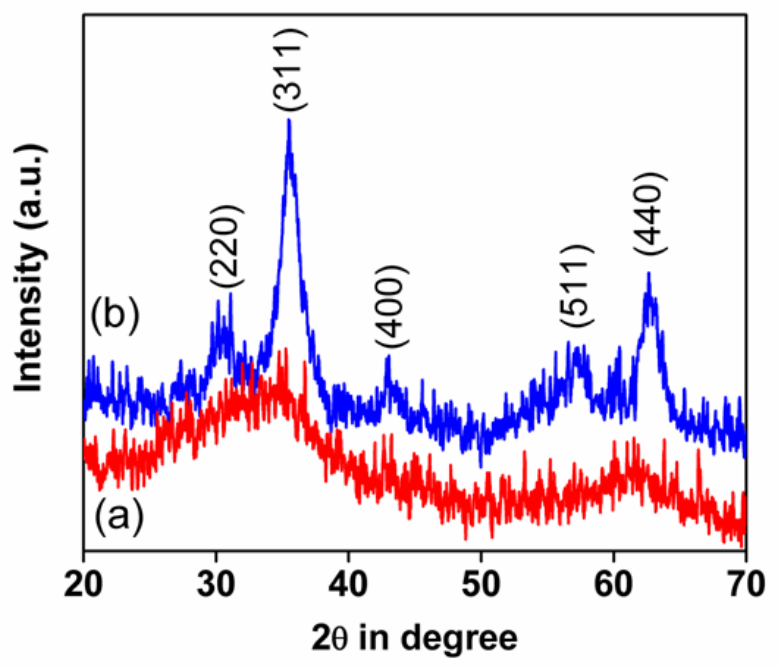

Figure S5: Wide angle powder X-ray diffraction patterns of Fe_3O_4@GO-1 (a) Fe_3O_4@GO-2 (b) nanocatalysts, respectively.

Wide angle powder X-ray diffraction patterns of Fe_3O_4@GO nanocatalysts are provided in Figure S5. Fe_3O_4@GO-2 nanocatalyst displayed (Figure S5b) well resolved characteristic diffraction peaks at the 2θ values 30.3, 35.4, 42.9, 57.3 and 62.6, respectively corresponding to the crystalline reflection patterns (220), (311), (400), (511) and (440), respectively which can be readily indexed to the with the face centered cubic lattice (fcc) crystal structure model (JCPDS card no. 19-0629) of Fe_3O_4 nanoparticles.[2] But Fe_3O_4@GO-2 demonstrates (Figure S5a) poor crystalline feature or the small crystal domain in the product, which is the outcome of less reaction time during the synthesis procedure.

Section S8: XPS survey spectra of Fe_3O_4@GO nanocatalysts

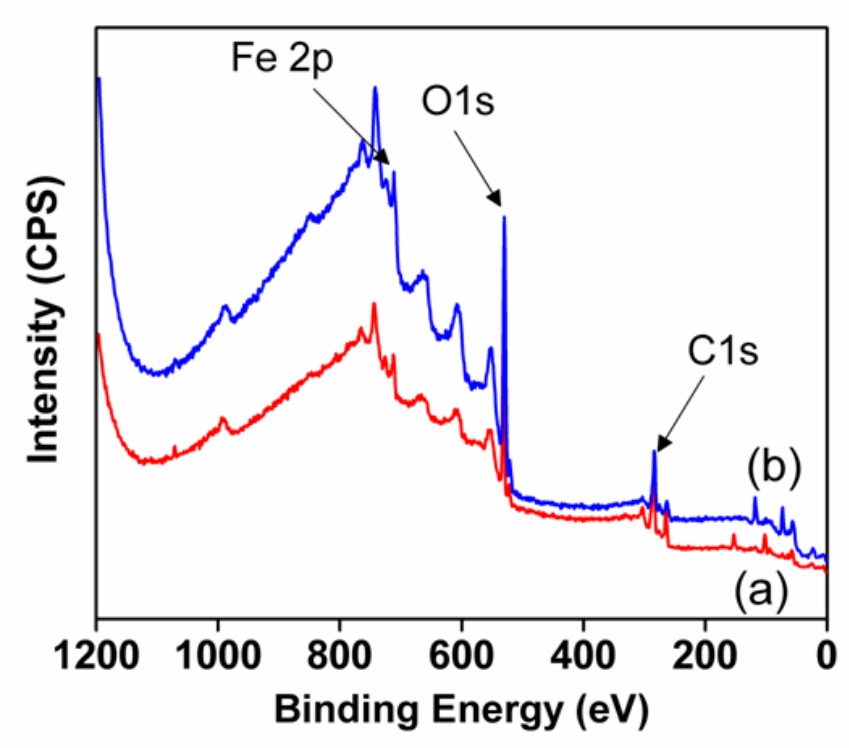

Figure S6: XPS survey spectra of Fe_3O_4@GO-1 (a) Fe_3O_4@GO-2 (b) nanocatalysts, respectively

Section S9: C1s XPS spectra of Fe_3O_4@GO nanocatalysts

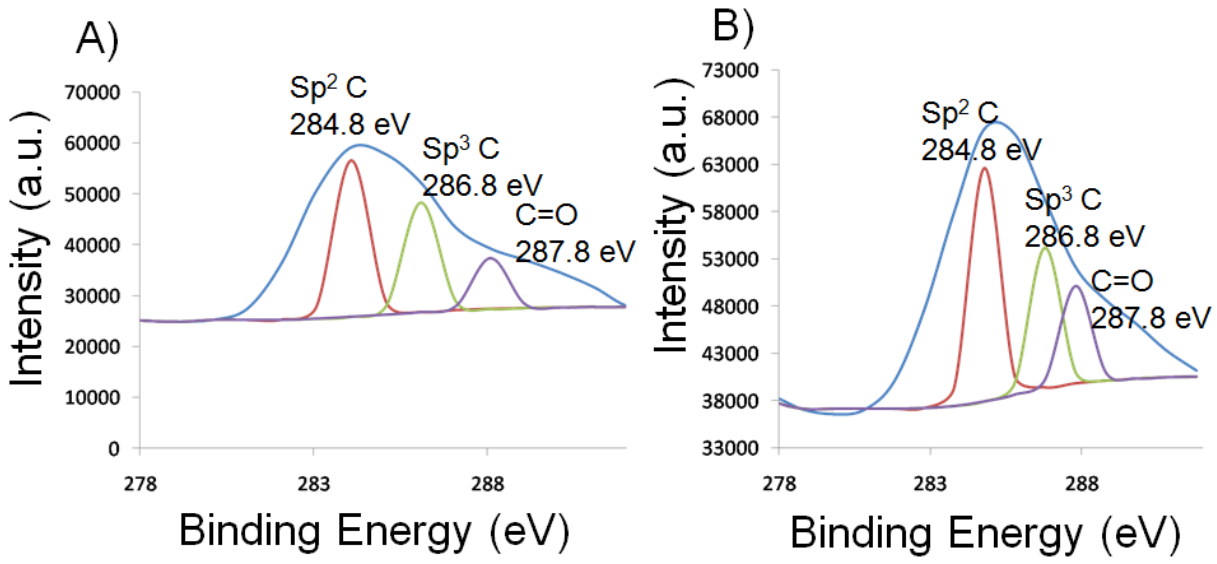

Figure S7: C1s XPS spectra of Fe_3O_4@GO-1 (A) and Fe_3O_4@GO-2 (B) nanocatalysts, respectively.

C1s XPS spectra of Fe_3O_4@GO nanocatalysts are given in the Figure S7. The C1s XPS spectra (Figure S7A & S7B) of the both catalysts display three binding energy peaks centered at 284.8 eV, 286.8 eV and 287.8 eV, attributed to the three components C-C, C-O carbons and C=O carbon atoms of graphene oxide, respectively.[3] The binding energy peaks of $Fe2p_{3/2}$ and $Fe2p_{1/2}$ in Fe_3O_4@GO-2 was observed at 711.5 eV and 725.2 eV (Figure 1C Main manuscript). Similarly, the peaks positioned at 711.4 eV and 724.8 eV in Figure 1C was observed for Fe_3O_4@GO-1. The values obtained match well with the reported literature values. Observed Fe $2p_{3/2}$ BE peak was well distinguished from Fe $2p_{3/2}$ of FeO (709.4 eV) and Fe_2O_3 (710.8 eV).

Section S10: FT-IR spectra of Fe_3O_4@GO nanocatalysts

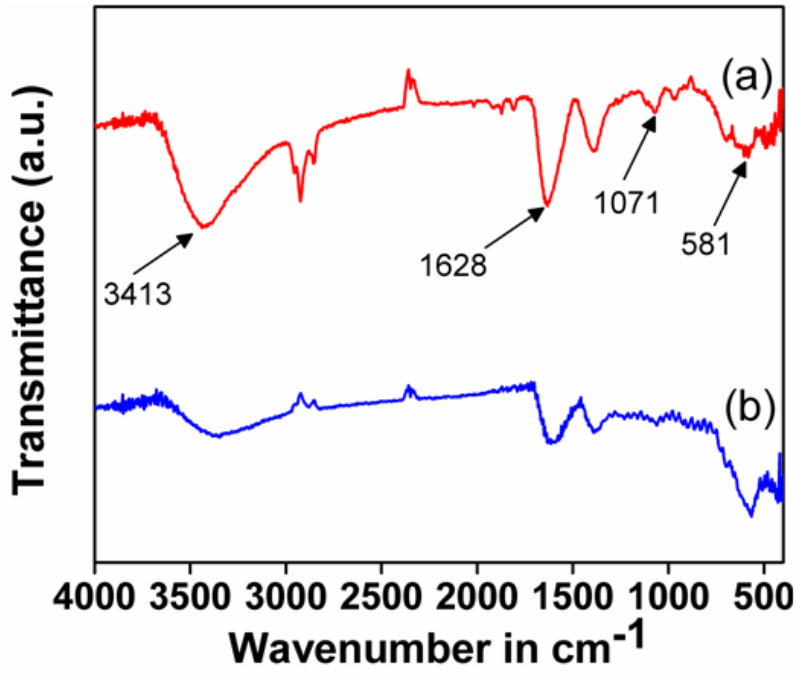

Figure S8: FT-IR spectra of Fe_3O_4@GO-1 (a) Fe_3O_4@GO-2 (b) nanocatalysts, respectively.

FT-IR spectra of Fe_3O_4@GO nanocatalysts are provided in the Figure S8. The board band centered at 3413 cm^{-1} that can be attributed to the O-H stretching vibration of graphene oxide. FT-IR spectrum of Fe_3O_4@GO (Figure S8) displays peak at 1628 cm^{-1}, which can be assigned to the stretching frequency of C=O bond. The stretching frequency of epoxy vibration of graphene oxide unit arises at 1071 cm^{-1}. IR spectra show strong absorption band at 581 cm^{-1} ascribed to the $\upsilon_{Fe\text{-}O}$ in Fe_3O_4 nanoparticles.[4a]

Section S11: Dynamic Light Scattering Spectra of Fe_3O_4@GO nanocatalysts

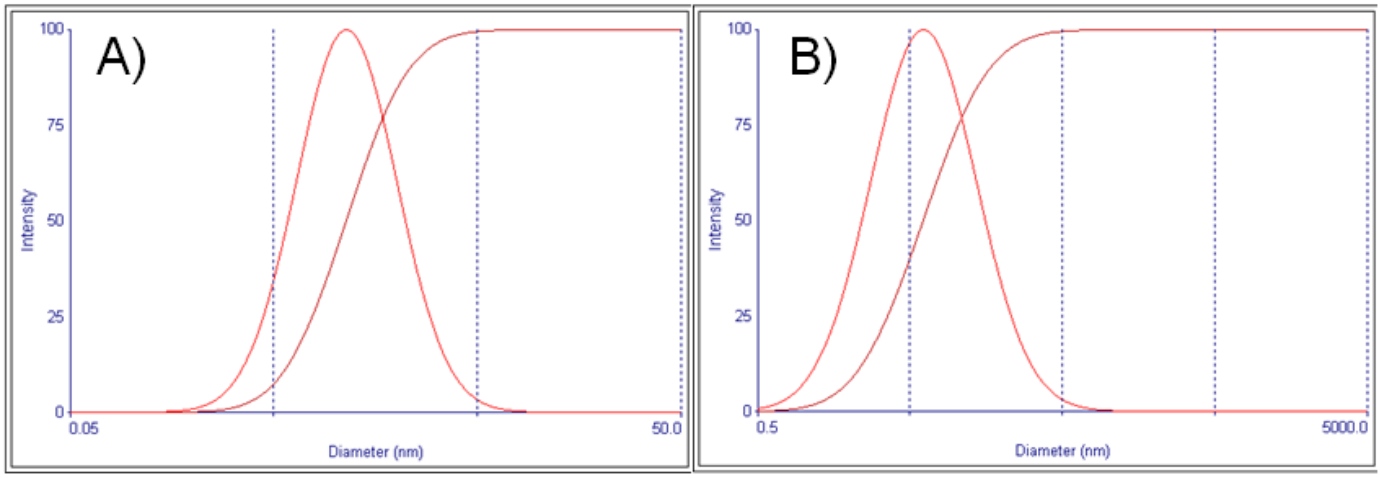

Figure S9: Dynamic Light Scattering spectra of Fe_3O_4@GO-1 (A) Fe_3O_4@GO-2 (B) nanocatalysts, respectively.

Section S12: Atomic force microscopy spectra of Fe_3O_4@GO nanocatalysts

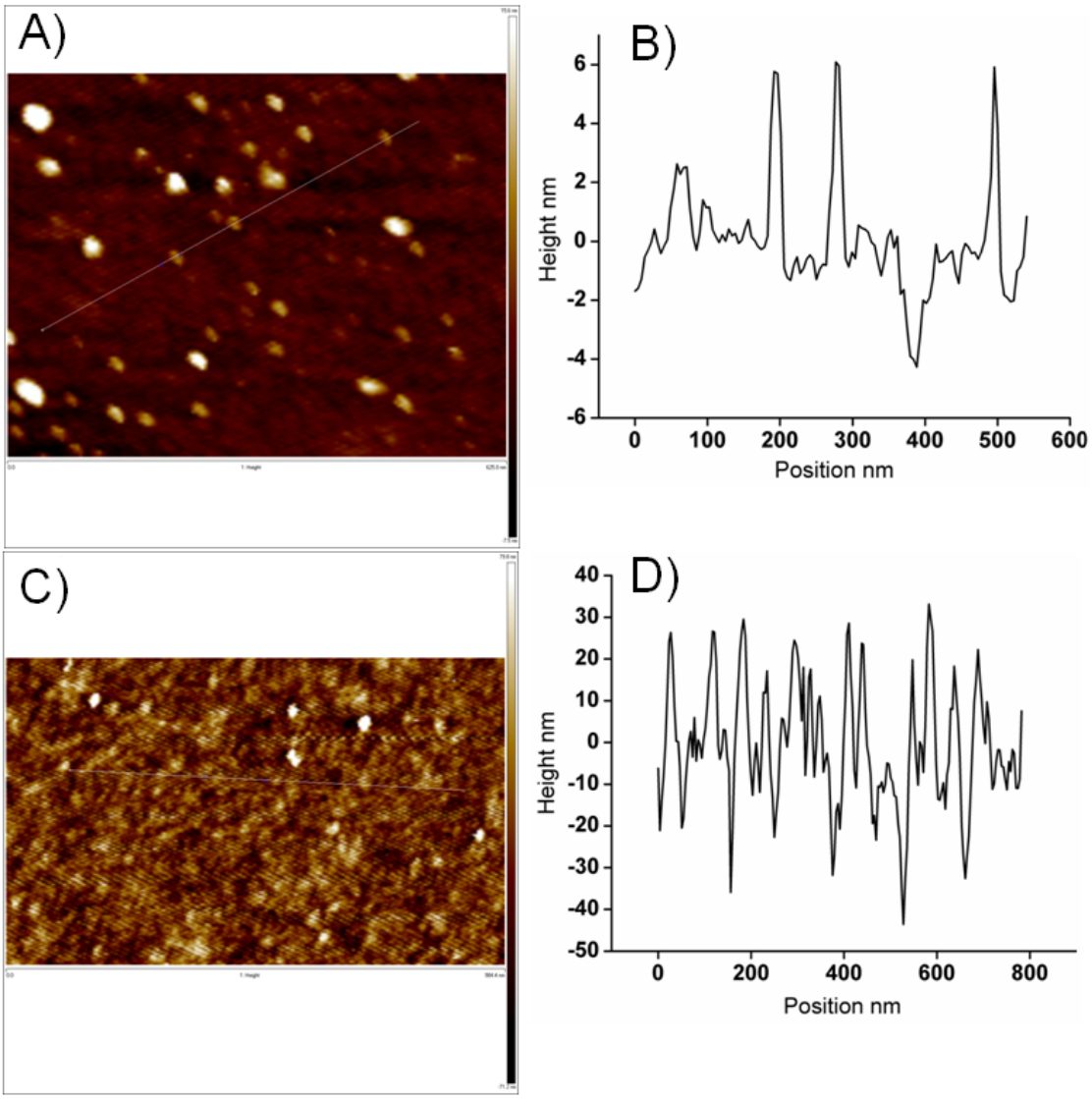

Figure S10: AFM topography images of Fe_3O_4@GO-1 (A) Fe_3O_4@GO-2 (C) nanocatalysts and cross sections along the two directions marked in the topography images (B) and (D), respectively.

Atomic Force Microscopy technique was carried out in order to take a view the cross sectional features of our newly developed Fe_3O_4@GO nanocatalysts. The AFM topography image of Fe_3O_4@GO-1 nanocatalyst is provided in the Figure S10A. The bright color particles signify that the height is greater compared with the other nanoparticles. The white line which is drawn on the AFM image suggests the vertical cross sectional of height profile of nanoparticles which are embedded on the surface of graphene oxide material. This height profile shows the topography variation over nanoparticles on the graphene oxide surface. We have drawn a corresponding cross sectional topography graph which is given in the Figure S10B. The same thing we have carried out for Fe_3O_4@GO-2 nanocatalyst. The AFM topography image and the corresponding topography graph are provided in the Figure S10C and S10D, respectively.[4b]

Table S1: Optimization table of alkene hydrogenation reaction with Fe_3O_4@GO nanocatalyst[a]

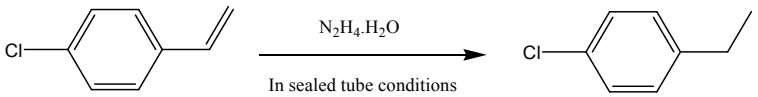

Entry	Hydrogen source	Solvent	Time (hr)	Conversion[b] (%)
1	No Additive	EtOH	20	0
2	$N_2H_4.H_2O$ (1.5 equiv)	EtOH	4	20
3	$N_2H_4.H_2O$ (3.0 equiv)	EtOH	4	22
4	$N_2H_4.H_2O$ (4.0 equiv)	EtOH	4	45
5	$N_2H_4.H_2O$ (5.0 equiv)	EtOH	4	58
6	$N_2H_4.H_2O$ (6.0 equiv)	EtOH	4	69
7	$N_2H_4.H_2O$ (8.0 equiv)	EtOH	4	78
8	**$N_2H_4.H_2O$ (10.0 equiv)**	**EtOH**	**4**	**99**
9	$N_2H_4.H_2O$ (10.0 equiv)	EtOH	10	70
10[c]	$N_2H_4.H_2O$ (10.0 equiv)	Toluene	12	30
11[d]	$N_2H_4.H_2O$ (10.0 equiv)	DMF	12	45
12[e]	$N_2H_4.H_2O$ (10.0 equiv)	DMSO	12	50
13[f]	$N_2H_4.H_2O$ (10.0 equiv)	THF	12	26
14[g]	$N_2H_4.H_2O$ (10.0 equiv)	H_2O	12	14
15[h]	$N_2H_4.H_2O$ (10.0 equiv)	EtOH	20	40

[a]Reaction conditions: 4-chlorostyrene (0.25 mmol, 0.034g), catalyst (15 mg), $N_2H_4.H_2O$ (10 equivalent, 2.5 mmol, 125 mg), EtOH (3 mL), 80°C; [b]Determined by GC analysis using dodecane as GC internal standard; [c]Toluene (3 mL), 110°C; [d]DMF (3 mL), 110°C; [e]DMSO (3 mL), 110°C; [f]THF (3 mL), 60°C; [g]H_2O (3 mL), 110°C; [h]Reaction was carried out at room temperature (25°C).

We have employed our newly developed Fe_3O_4 nanoparticles embedded in graphene oxide nanocatalysts to carry out hydrogenation reaction using hydrazine hydrate as hydrogen source. For the optimization of reaction conditions we have started our initial study with the catalytic reaction of 4-chlorostyrene (0.25 mmol) in EtOH (4 mL) and Fe_3O_4@GO-2 catalyst (15 mg) in a

sealed tube at 80°C (oil bath). In the absence of any additive (external hydrogen source) no catalytic conversion took place (Table S1, entry 1). Then we have used hydrazine hydrate ($N_2H_4.H_2O$) as external hydrogen source for hydrogenation of 4-chlorostyrene. Initially we have used 1.5 equivalent of $N_2H_4.H_2O$ which gave us only 20% product conversion (Table S1, entry 2). Then we have started to increase gradually the amount of $N_2H_4.H_2O$ (from 3.0 equivalents to 10.0 equivalents) then the catalytic reactions proceed faster (Table S1, entries 3-7). 10.0 equivalents $N_2H_4.H_2O$ is quite enough to complete the reduction of without leaving any trace of incomplete reduction products (Table S1, entry 8). Fe_3O_4@GO-1 nanocatalyst showed poor conversion compared with the Fe_3O_4@GO-2 nanocatalyst keeping other parameters same (Table S1, entry 9). When the catalytic hydrogenation reaction was conducted in non-polar solvent like toluene 30% conversion of desired product was obtained (Table S1, entry 10). When polar aprotic solvents like DMF and DMSO were employed as solvents (Table S1, entries 11 & 12), 45%-50% conversion of desired product have been achieved. However, tetrahydrofuran (THF) has been also considered as poor solvent for this alkene hydrogenation reaction (Table S1, entry 13) presumably owing to the lower reaction temperature. Refluxing in aqueous medium delivered even lower conversion of product (Table S1, entry 14). Temperature plays a crucial role for carrying out the catalytic alkene hydrogenation reaction. At room temperature, only 40% product conversion has been achieved after 20 h using Fe_3O_4@GO-2 as catalyst (Table S1, entry 15).

Table S2: Screening of different catalysts for alkene hydrogenation reaction under optimized reaction conditions[a]

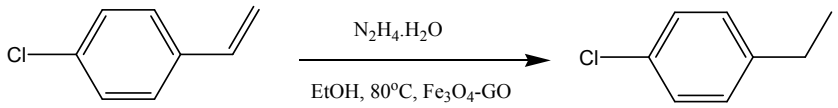

Entry	Catalyst	Time (h)	Conversion[b] (%)
1	Fe_3O_4 nano	16	45
2	Graphene oxide	20	0
3	Fe_3O_4@GO-1	4	70
4	Fe_3O_4@GO-2	4	99
5[c]	Fe_3O_4@GO-2	4	40
6[d]	Fe_3O_4@GO-2	4	25
7[e]	Fe_3O_4@GO-2	4	99
8[5]	Fe_3O_4 (40 mol%)	16	99
9[6]	Cu/DH	8	99
10[1a]	Fe-NP/CDG	24	99
11[f]	Fe_3O_4-GO	16	90
12[g]	Fe_3O_4@GO-2	16	18
13	Pd/C	12	50

[a]Reaction conditions: 4-chlorostyrene (0.25 mmol, 0.034g), catalyst (15 mg), $N_2H_4.H_2O$ (10 equivalent, 2.5 mmol, 125 mg), EtOH (3 mL), 80°C; [b]Determined by GC analysis using dodecane as GC internal standard; [c]4.9×10^{-4} mol% catalyst loading; [d]2.46×10^{-4} mol% catalyst loading; [e]9.85×10^{-4} mol% catalyst loading. [f]Fe_3O_4 nanoparticles are externally mixed with GO; [g]No stirring bar was used.

In order to evaluate catalytic activity of Fe_3O_4@GO-2 nanocatalyst with different catalyst loading (mol%) we have carried out the catalytic alkene hydrogenation reaction of 4-chlorostyrene under optimized reaction conditions. When bare Fe_3O_4 nanoparticles have been used to carry out this reaction it provided 45% product conversion after 16 hr (Table S2, entry 1). Only GO showed no catalytic activity for this catalytic alkene hydrogenation reaction (Table S2, entry 2). But when Fe_3O_4@GO nanocomposites have been used as catalysts to carry out this hydrogenation reaction then the reaction was finished at 10 hr and 4 hr providing 70% and 99% conversions, respectively (Table S2, entries 3 & 4). This result clearly proves that GO has a decisive role for this alkene hydrogenation reaction using *in situ* hydrogen generation technique. Strong adsorption of organic molecules onto graphene oxide sheet is attributed to the π stacking and hydrophobic interactions that renders enhancement of catalytic conversion of Fe_3O_4@GO nanocatalyst. Catalytic activity appeared to be dependent on the catalytic dose (mole % loading of Fe) which has been proved by conducting reaction with different catalyst loading. The reaction with 10 mg (4.9×10^{-4} mol% catalyst loading) and 5 mg (2.46×10^{-4} mol% catalyst loading) catalysts afforded 40% and 25% conversions, respectively (Table S2, entries 5 & 6). But no substantial change in the product conversion was observed with the increase of the catalyst dose (Table S2, entry 7). Hence, we can conclude that 15 mg is the optimum amount of catalyst required to carry out this catalytic alkene hydrogenation reaction. In the previously published results predict that 40 mol% F_3O_4 nanoparticles (very high catalyst loading) have been used as catalyst to carry out this catalytic hydrogenation reaction which provides 99% conversion requiring 16 hr reaction time. The catalytic performance of Cu/DH and Fe-NP/CDG catalysts were also evaluated. The very high TOF (33482.1 h^{-1}) for the Fe_3O_4@GO-2 catalyst with 0.1232 μmol/g Fe (Table S2 , entry 4) by far exceeds the TOFs for the same reaction

catalyzed by Fe_3O_4 (same loading) nanoparticles immobilized externally on the surface of GO (7609.5 h^{-1}) (Table S2, entry 11). However, the conversion get dropped by five fold compared with the reaction with stirring bar (Table S2, entry 12). This fact predicts us that vigorous stirring using an internal stirring magnet, which is a key factor since hydrogen generation *in situ* with the contact of hydrazine monohydrate with graphene oxide area is essential for this reaction. We have also carried out the alkene hydrogenation reaction with Pd/C catalyst under this optimized condition which gave 50% product conversion (Table S2, entry 13).

Section S13: Comparative study on catalytic conversion

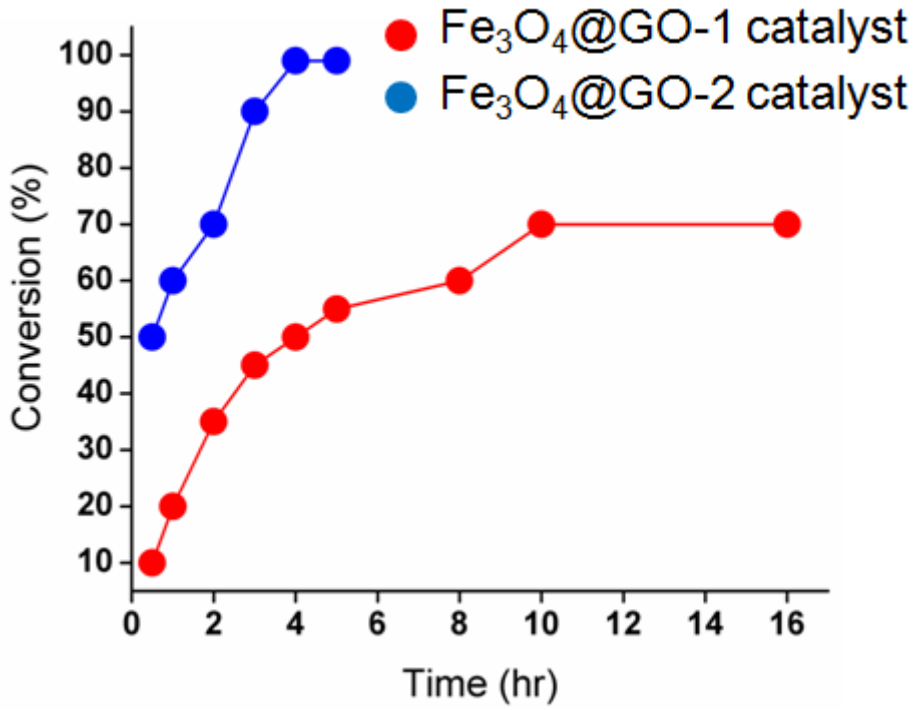

Figure S11: Comparative study on catalytic conversion over two different Fe_3O_4@GO catalysts.

We have carried out comparative study on catalytic conversion of 4-Chlorostyrene against time (hr) employing two different Fe_3O_4@GO nanocatalysts. We have performed the reaction considering 4-Chlorostyrene as model substrate under optimized reaction conditions. After each interval time (hr) we have separated the catalyst by magnetic separation and reaction mixture was analyzed by GC-MS and GC tools to calculate the conversion (%). From the Figure S11 it is quite evident that conversion (%) for Fe_3O_4@GO-2 has been increased against time (hr) and is finished at 4 hr. After 5 hr we got the same conversion (%). But in case of Fe_3O_4@GO-1 nanocatalyst we have achieved 70% conversion after 10 hr. Then with the increase of time (hr) no improvement of conversion (%) has been reached. From these results we can conclude that

large Fe_3O_4 nanoparticles (15 nm size) with high crystalline feature embedded on graphene oxide support for Fe_3O_4@GO-2 are more beneficial for the catalytic transfer hydrogenation reaction from hydrazine hydrate in EtOH medium.

Section S14: Reusability of Fe_3O_4@GO-2 nanocatalyst

Magnetic separation is a more attractive and simple technique than the filtration or centrifugation techniques as it prevents the loss of the catalyst and increases the reusability of the catalyst. Due to the superparamagnetic nature of Fe_3O_4 nanoparticles at room temperature separation of the Fe_3O_4@GO-2 nanocatalyst from the reaction mixture becomes very easy. In the magnetic separation technique the catalyst became adsorbed onto the magnetic stirring bar when the stirring was stopped. Then the catalyst was washed with acetone, oven dried (80^{o}C temperature) and then directly used for the next cycle reaction without further purification. A recyclability test was performed by considering alkene hydrogenation reaction of 4-methylstyrene using hydrazine hydrate as a model reaction. Recyclable potential plot of Fe_3O_4@GO-2 nanocatalyst suggested that the nanocatalyst can be effectively reused for ten consecutive catalytic cycles (ESI, Fig. S12). A slight drop in the conversion (%) from the 8th to 10th cycles is observed which is due to the clogging of some catalytic active sites with organic reagents during the course of reaction. In every case our recovery of catalyst from the reaction mixture is almost 100%. We have also provided the distribution of product yield which remains consistent in each catalytic cycle.

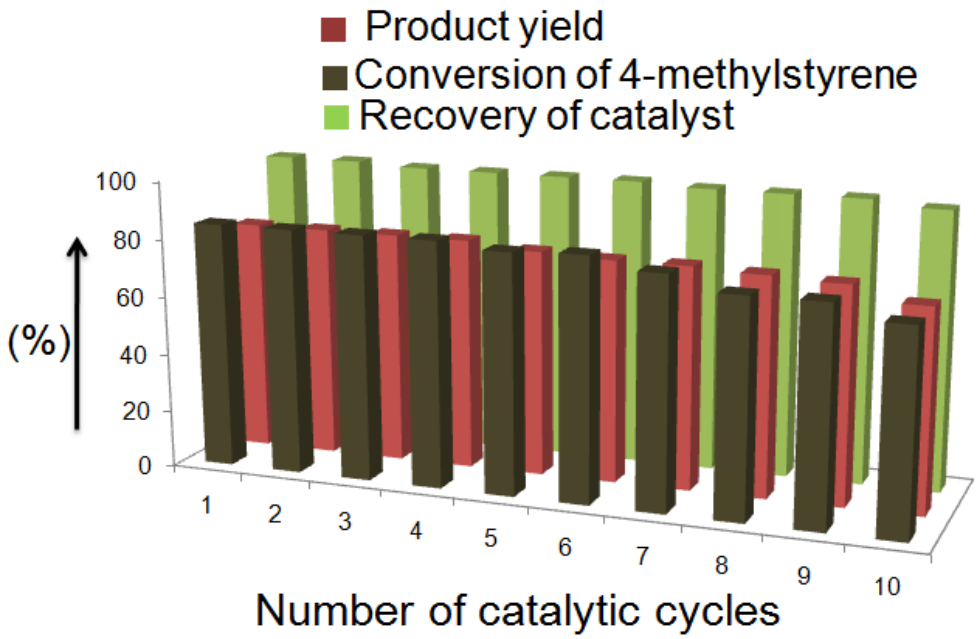

Figure S12: Recycling efficiency of Fe_3O_4@GO-2 nanocatalyst for several reaction cycles.

Section S15: Leaching and hot filtration test

Leaching test: AAS (Atomic Absorption Spectroscopy) technique was employed to be sure that no leaching of Fe took place after 10th catalytic reaction. After the completion of reaction, the Fe_3O_4@GO-2 nanocatalyst was separated using a stirring magnet and washed with acetone, dried in oven. The filtrate (reaction mixture) was analyzed using AAS (Atomic Absorption Spectroscopy) analysis which indicates that no Fe was detected in the filtrate solution. One important point should be noticed that the filtrate remains complete colorless. The experimental data clearly demonstrates that the Fe_3O_4 nanoparticles were strongly embedded on the graphene oxide sheet, and no leaching of Fe from the nanocatalyst took place during the course of hydrogenation reaction.

Hot filtration test: We have carried out the hot filtration test to investigate heterogeneous nature of Fe_3O_4@GO-2 nanocatalyst and to make sure no leaching of Fe during the course of catalytic alkene hydrogenation reaction. In this test, a mixture of Fe_3O_4@GO-2 (15 mg), 4-methylstyrene (0.25 mmol, 0.034g), $N_2H_4.H_2O$ (2.5 mmol, 125 mg), in EtOH (3 mL) was heated at 80^{o}C for 6 h. The Fe_3O_4@GO-2 catalyst was separated from the hot reaction mixture after 6 h using magnetic separation technique. Then, it was observed by using GC that only 50% conversion was achieved. The reaction was continued with the filtrate for another 6 h at the same reaction temperature. But, no increase in the hydrogenation product conversion was observed after 6 hr confirmed by GC analysis. After the completion of the reaction, no detectable leaching of iron was found by AAS analysis.

Section S16: Characterization of Reused catalyst

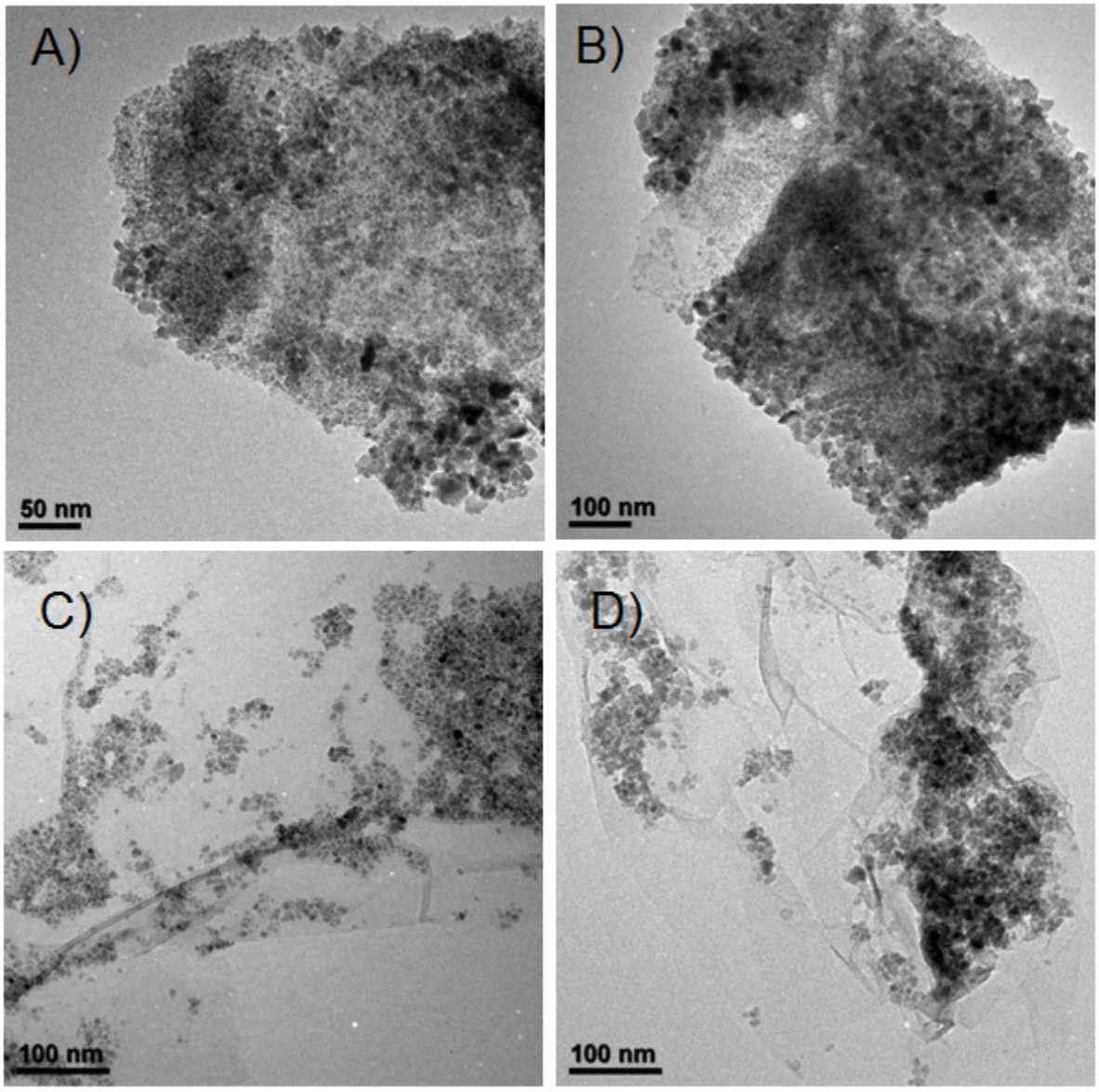

Figure S13: TEM images (A), (B) after 6th and (C), (D) after 10th catalytic cycles of Fe_3O_4@GO-2 nanocatalyst.

We have characterized our reused Fe_3O_4@GO-2 nanocatalyst after 6th and 10th catalytic cycles using TEM image analysis in order to confirm mechanical and thermal stability of reused catalyst after several catalytic reactions. Figure S13 indicates that the black color 15 nm Fe_3O_4 nanoparticles are homogeneously distributed throughout the graphene oxide surface after the 6th and as well as 10th catalytic cycles. Then we have carried out XPS analysis to confirm that oxidation state of Fe remains unaltered after the 10th catalytic cycles of the reactions. Figure S14A XPS spectrum of Fe 2p region signifies that the oxidation state of Fe remains unchanged during the course of reaction and after reaction. Raman spectrum of reused Fe_3O_4@GO-2 nanocatalyst is given in the Figure S14B. I_D/I_G for this reused Fe_3O_4@GO-2 nanocatalyst is 1.05 remains unaltered which suggests that our catalyst is exceptionally stable after the catalytic reactions. Atomic Force Microscopy topography image and the corresponding cross sectional feature of the reused Fe_3O_4@GO-2 nanocatalyst after 10th catalytic cycles are provided in the Figure S14C & D which suggest that catalyst surface and cross section feature remains unaltered after the catalytic reaction.

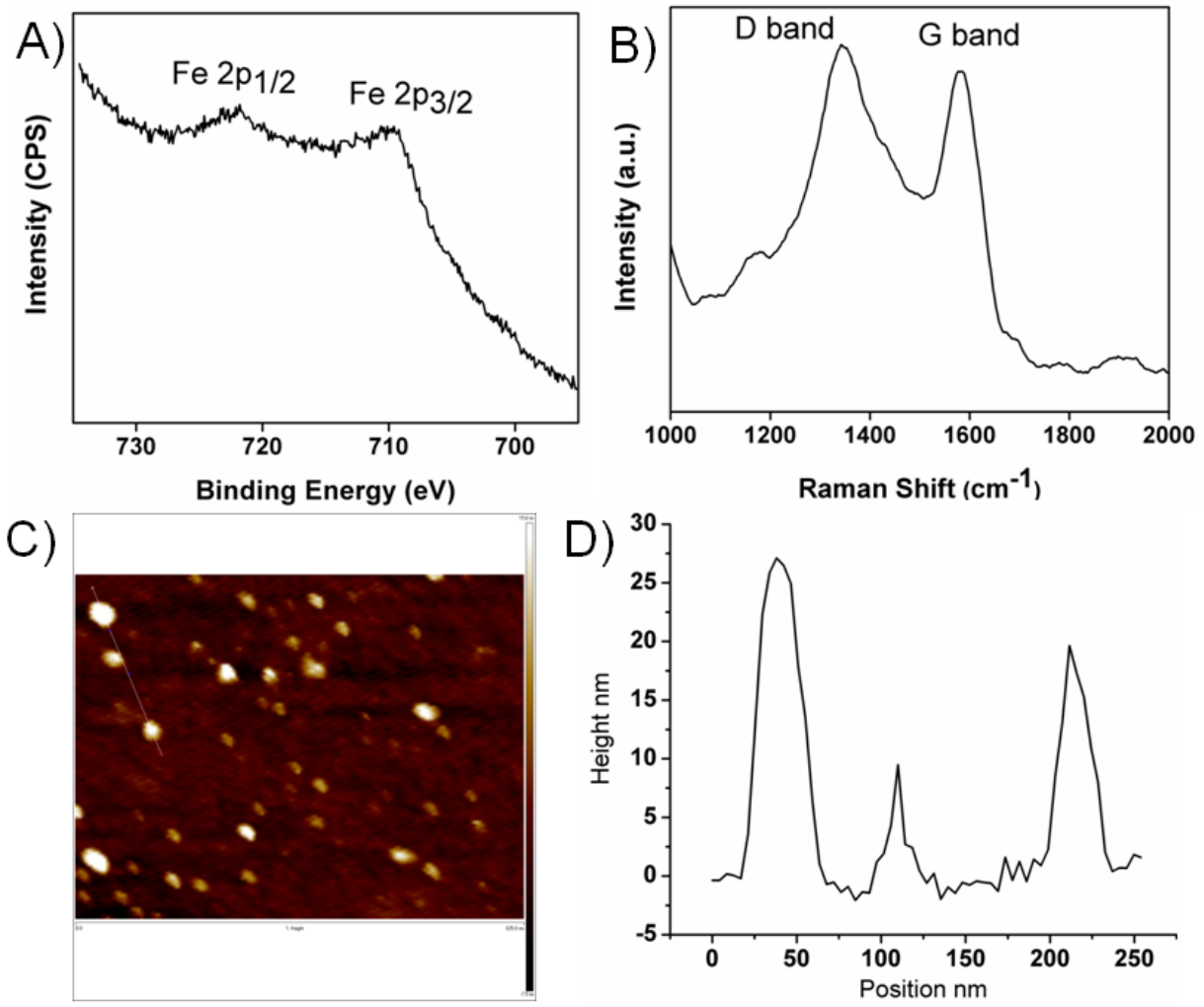

Figure S14: (A) XPS spectrum of Fe 2p region, (B) Raman spectrum, (C) AFM topography image and (D) corresponding cross sectional pattern of reused Fe_3O_4@GO-2 nanocatalyst after 10^{th} catalytic cylces.

Section S17: Plausible Reaction pathway

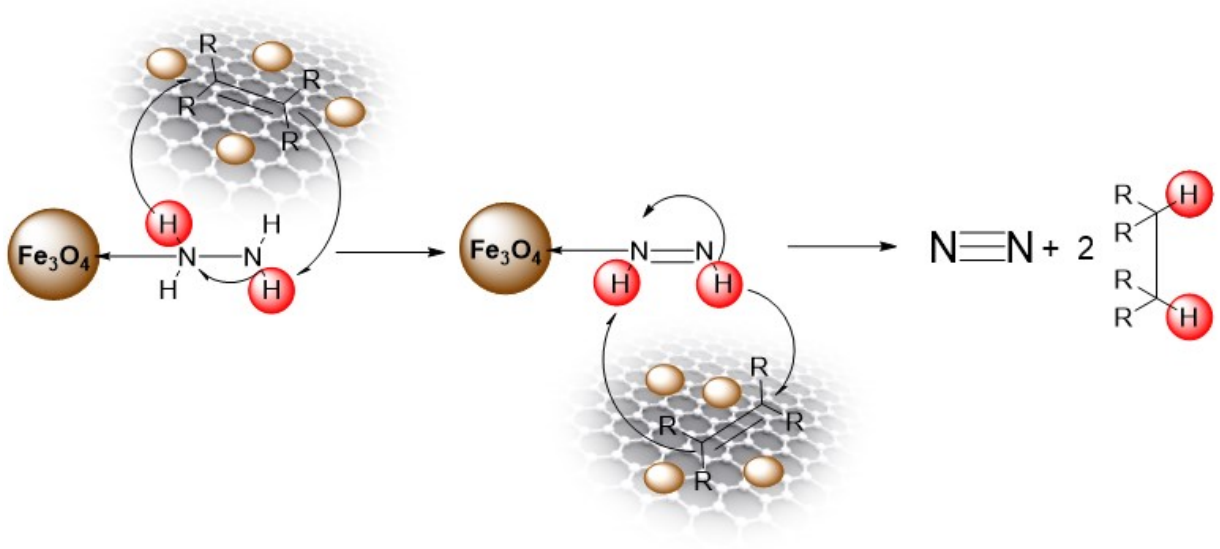

Figure S15: Plausible reaction pathway for catalytic alkene hydrogenation with Fe_3O_4@GO nanocatalyst

We have provided the possible reaction pathway for this alkene hydrogenation reaction over Fe_3O_4@GO nanocatalyst in the Figure S15. According to our proposed plausible reaction pathway it is suggested that $N_2H_4.H_2O$ gets dissociated on the external surface of Fe_3O_4 nanoparticles into N_2 and H_2. First alkenes are adsorbed on the surface of graphene oxide owing to the π-π stacking and hydrophobic interactions. Then N atom of $N_2H_4.H_2O$ is coordinated with the Fe_3O_4 making N atom more + ve charge. It is expected that hemolytic cleavage of N-H bond took place and thereby H' radical is transferred to alkenes. Then the sequential transfer of H' radical in the similar fashion from H-N=N-H intermediate took place and N_2 is liberated leading to the formation of corresponding alkanes.

Section S18: References

(1)	(*a*) M. Stein, J. Wieland, P. Steurer, F. Tçlle, R. Mulhaupt and B. Breit, *Adv. Synth. Catal*., 2011, **353**, 523-527; (*b*) X. Huo, J. Liu, B. Wang, H. Zhang, Z. Yang, X. Sheb and P. Xia, *J. Mater. Chem. A*, 2013, **1**, 651-656; (*c*) K. Turcheniuk, M. Khanal, A. Motorina, P. Subramanian, A. Barras, V. Zaitsev, V. Kuncser, A. Leca, A. Martoriati, K. Cailliau, J-F. Bodart, R. Boukherroub and S. Szunerits, *RSC Adv*., 2014, **4**, 865-875; (*d*) J. Liu, Z. Sun, Y. Deng, Y. Zou, C. Li, X. Guo, L. Xiong, Y. Gao, F. Li and D. Zhao, *Angew. Chem., Int. Ed*., 2009, **48**, 5875-5879; (*e*) X. Jia, D. Chen, X. Jiao and S. Zhai, *Chem. Commun*., 2009, 968–970.
(2)	Y. Deng, D. Qi, C. Deng, X. Zhang and D. Zhao, *J. Am. Chem. Soc*., 2008, **130**, 28 – 29.
(3)	(*a*) S. Zu and B. Han, *J. Phys. Chem. C*, 2009, **113**, 13651-13657; (*b*) J. I. Paredes, S. Villar-Rodil, A. Mart_ınez-Alonso and J. M. D. Tascon, *Langmuir*, 2008, **24**, 10560-10564.
(4)	(*a*) M. Ma, Y. Zhang, W. Yu, H. Y. Shen, H. Q. Zhang and N. Gu, *Colloids Surf., A*, 2003, **212**, 219 – 226; (*b*) K. T. Nguyen, S. Sreejith, J. Joseph, T. He, P. Borah, E. Y. Guan, S. W. Lye, H. Sun and Y. L. Zhao, *Part. Part. Syst. Charact.*, 2014, DOI: 10.1002/ppsc.201400044.
(5)	E. Kim, S. Kim and B.M. Kim, *Bull. Korean Chem. Soc*., 2011, **32**, 3183-3186.
(6)	A. Dhakshinamoorthy, S. Navalon, D. Sempere, M. Alvaro and H. Garcia, *Chem. Commun.*, 2013, **49**, 2359-2361.